Article

Exploring the Exact Solution of the Space-Fractional Stochastic Regularized Long Wave Equation: A Bifurcation Approach

Bashayr Almutairi, Muneerah Al Nuwairan *[ID] and Anwar Aldhafeeri [ID]

Department of Mathematics and Statistics, College of Science, King Faisal University,
P.O. Box 400, Al-Ahsa 31982, Saudi Arabia; 222400521@student.kfu.edu.sa (B.A.); aaaldhafeeri@kfu.edu.sa (A.A.)
* Correspondence: msalnuwairan@kfu.edu.sa

Abstract: This study explores the effects of using space-fractional derivatives and adding multiplicative noise, modeled by a Wiener process, on the solutions of the space-fractional stochastic regularized long wave equation. New fractional stochastic solutions are constructed, and the consistency of the obtained solutions is examined using the transition between phase plane orbits. Their bifurcation and dependence on initial conditions are investigated. Some of these solutions are shown graphically, illustrating both the individual and combined influences of fractional order and noise on selected solutions. These effects appear as alterations in the amplitude and width of the solutions, and as variations in their smoothness.

1. Introduction

The long wave equation is a well-known model for studying shallow water environments. It is a mathematical model that describes the propagation of long waves in certain physical systems. It is used in modeling various natural phenomena characterized by weak non-linearity and dispersive waves, and was introduced by Peregrine [1] to describe the development of an undular bore. The authors in [2] examined the equation as an extension of the Kortewe–de Vries equation (KdV equation) to model small-amplitude, long surface gravity waves propagating in one spatial dimension. The regularized long wave (RLW) equation is a modified version of the long wave equation that includes regularization terms to account for wave dispersion and improve the accuracy of wave propagation modeling [2]. It is given by the following equation:

$$\mathcal{Q}_t + \mathcal{Q}_x - \frac{m}{2}\mathcal{Q}\mathcal{Q}_x - n\mathcal{Q}_{xxt} = 0, \tag{1}$$

where m and n are free constants that control the nonlinear and dispersive effects, respectively. Here, $\mathcal{Q}(x,t)$ is the amplitude of the wave function, with t and x being the temporal and spatial variables, respectively.

The equation in (1) can be used to model a variety of phenomena in physics, including ion-acoustic plasma waves, dissipative processes in heat conduction, and nonlinear wave diffusion. The behavior of the RLW equation is influenced by the values of parameters m and n. For instance, if $m = 0$ and $n = 1$, then Equation (1) becomes a linear wave equation, which describes the behavior of waves with small amplitudes. If $m > 0$ and $n = 1$, it exhibits nonlinear behavior, indicating that the wave's amplitude can change as it propagates. For $n > 1$, it exhibits dispersive behavior, enabling the wave to modify its shape during propagation due to the variation in wave velocity with frequency. Many analytical and numerical methods were used to obtain solutions for Equation (1) in [3–6]. It is worth mentioning that soliton solutions arise from the balancing of the last two terms.

While classical differential equations have been successful in modeling a wide range of phenomena [7,8], there are many situations where they may not adequately capture the underlying dynamics, especially in systems with memory or inherited properties. Fractional differential equations (FDEs) [9,10] generalize classical differential equations by allowing non-integer order of derivatives, making them more flexible in modeling complex phenomena. Nonlinear FDEs offer more precise models for describing nonlinear systems in fields like fluid mechanics and signal processing. They have been employed in the analysis of complex physical and biological systems [11–14].

A different generalization of classical differential equations is stochastic differential equations (SDEs). The SDEs are suitable for modeling systems that are inherently random or are subject to random effects by adding a stochastic term that represents randomness in the system. Nonlinear stochastic differential equations are widely used in finance, biology, physics, and engineering [15–17]. In fact, in several scientific branches, there is a strong emphasis on incorporating random effects into the modeling, analysis, and simulation of complex phenomena. This is because noise can generate statistical properties and behavior that should not be overlooked [18,19]. Fractional derivatives are often preferred for modeling these phenomena over integer-order derivatives. Using both fractional and stochastic generalizations in one model offers a more flexible tool for modeling systems that exhibit both memory effects and randomness. Research on stochastic fractional differential equations (SFDEs) is a growing area in applied mathematics, e.g., [20–27].

Like most differential equations, the RLW has been generalized using different types of fractional derivatives, and methods to solve such generalizations were investigated [28–30].

In this study, we introduce a generalization of the RLW Equation (1) using Jumarie's modified Rieman–Liouville fractional derivative and stochastic process (see Appendix A), as follows:

$$
\mathrm{d}\mathcal{Q} + \left[\mathbb{T}_x^p \mathcal{Q} - \frac{m}{2} \mathcal{Q} \mathbb{T}_x^p \mathcal{Q} \right] \mathrm{d}t - n \mathbb{T}_x^{2p} \mathrm{d}\mathcal{Q} = \rho \left(\mathcal{Q} - n \mathbb{T}_x^{2p} \mathcal{Q} \right) \mathrm{d}\mathbb{H},
\tag{2}
$$

where $\mathbb{T}^p$ is the Jumarie's modified Rieman–Liouville fractional derivative of order p, ρ is the noise strength, $\mathbb{H}(t)$ is a white noise (Gaussian process), and $\mathcal{Q}\mathrm{d}\mathbb{H}$ is a multiplicative white noise in the Itô sense. Note that the noise-perturbed term is a combination of two terms appearing in [31,32].

Finding solutions for stochastic fractional partial differential equations poses a considerable challenge. In this paper, we explore the exact solutions of the SFRLW equation for different values of the controlling parameters m and n. Utilizing bifurcation theory, we introduce novel solutions, focusing exclusively on real solutions used in practical applications, particularly in the context of real wave propagation intervals. These solutions are novel even when compared to the deterministic form of Equation (2), whether featuring fractional or integer-order derivatives. We also explore the degeneracy of solutions to examine the consistency of obtained results and their dependence on initial conditions. Finally, we analyze the impact of noise and fractional-order derivatives on these solutions, both individually and together.

The layout of this paper is as follows: In Section 2, we derive a traveling wave system corresponding to the SFRLW Equation (2). The solution of this system plays an important role in the construction of the required solutions. Section 3 covers the bifurcation analysis for the traveling wave system and a concise explanation of the phase plane trajectories. In Section 4, we introduce some new solutions for the SFRLW Equation (2) and demonstrate the consistency of these solutions by studying the degeneracy property through transitions between phase plane orbits. In Section 5, the influence of both the fractional-order derivative and the noise strength, individually and in combination, on the obtained solutions is illustrated graphically. Section 6 summarizes the obtained results.

2. Mathematical Analysis

We seek solutions for Equation (2) of the form

$$\mathcal{Q}(x,t) = M(\xi)e^{\rho\mathbb{H}(t)-\frac{\rho^2}{2}t}, \xi = \frac{kx^p}{\Gamma(p+1)} + \omega t, \tag{3}$$

where k, ω are arbitrary constants and $\Gamma(\cdot)$ is the Gamma function [33]. After some computations, we obtained

$$d\mathcal{Q} = e^{\rho\mathbb{H}(t)-\frac{\rho^2}{2}t}\left[\omega M' dt + M\left(\rho d\mathbb{H} + \frac{\rho^2}{2} - \frac{\rho^2}{2}\right)\right], \tag{4a}$$

$$\mathbb{T}_x^p \mathcal{Q} = ke^{\rho\mathbb{H}(t)-\frac{\rho^2}{2}t} M', \tag{4b}$$

$$\mathbb{T}_x^{2p} \mathcal{Q} = k^2 e^{\rho\mathbb{H}(t)-\frac{\rho^2}{2}t} M'', \tag{4c}$$

$$\mathbb{T}_x^{2p} d\mathcal{Q} = k^2 [\omega M''' dt + \rho M'' d\mathbb{H}]e^{\rho\mathbb{H}(t)-\frac{\rho^2}{2}t}, \tag{4d}$$

where $'$ indicates derivatives with respect to ξ and $+\frac{\rho^2}{2}M$ in Equation (4a) is the Itô correction term. Substituting the expressions in Equation (4) into Equation (2), we obtain

$$-n\omega k^2 M''' - \frac{mk}{2}MM'e^{\rho\mathbb{H}(t)}e^{-\frac{\rho^2}{2}t} + (\omega + k)M' = 0. \tag{5}$$

Since $\mathbb{H}(t)$ is a Gaussian process, we have $\mathbb{E}\left(e^{\rho\mathbb{H}(t)}\right) = e^{\frac{\rho^2}{2}t}$. By equating the expectation on both sides of Equation (5), we obtain

$$-n\omega k^2 M''' - \frac{mk}{2}MM' + (\omega + k)M' = 0. \tag{6}$$

Integrating both sides of Equation (6) with respect to ξ, we have

$$M'' + 3\alpha M^2 - 2\beta M = 0, \tag{7}$$

where α and β are given by

$$\alpha = \frac{m}{12n\omega}, \beta = \frac{\omega + k}{2n\omega k^2}. \tag{8}$$

The integration constant is taken to be zero since it can be reduced to 0 by relocating the coordinate's origin.

Equation (7) can be expressed as a Hamiltonian system in the form

$$\begin{aligned} M' &= N, \\ N' &= M(2\beta - 3\alpha M), \end{aligned} \tag{9}$$

with the Hamiltonian function

$$H = \frac{1}{2}N^2 + \alpha M^3 - \beta M^2, \tag{10}$$

by using Hamilton's canonical equations [34,35]. Since H does not explicitly depend on ξ, the Hamiltonian function (10) is a constant of the motion. Thus, we have

$$\frac{1}{2}N^2 + \alpha M^3 - \beta M^2 = f, \tag{11}$$

where f is a free constant. Thus, constructing the solution to the SFRLW equation reduces to finding those of the Hamiltonian system (9), which describes motion in one dimension under the two parameters potential function

$$\mathcal{U} = \alpha M^3 - \beta M^2. \tag{12}$$

Inserting expression (9) into the constant of the motion (11) and separating the variables, we obtain

$$\frac{\mathrm{d}M}{\sqrt{\mathcal{W}_3(M)}} = \mathrm{d}\xi, \tag{13}$$

where $\mathcal{W}_3(M)$ is a cubic polynomial of the form:

$$\mathcal{W}_3(M) = 2\left[f + \beta M^2 - \alpha M^3\right]. \tag{14}$$

Integrating both sides of Equation (13) requires knowledge of the full range of parameters f, α, β. One method to determine this range is through the application of bifurcation theory [36].

3. Bifurcation Analysis

This section focuses on studying the bifurcation of the Hamiltonian system (9). The equilibrium points are the critical points for the potential function (12), i.e., $(M_0, 0)$, where M_0 is the solution $M_0(2\beta - 3\alpha M_0) = 0$. Thus, the equilibrium points are $A = (0, 0)$ and $B = \left(\frac{2\beta}{3\alpha}, 0\right)$. According to Lagrange's theorem [37], the equilibrium points are categorized based on whether they are maxima or minima of the potential function (12). We clearly have

$$\frac{d^2\mathcal{U}}{dM^2}(A) = -2\beta, \quad \frac{d^2\mathcal{U}}{dM^2}(B) = 2\beta. \tag{15}$$

When $\beta > 0$, the equilibrium point A is a saddle point and B is a center point. Likewise, when $\beta < 0$, A is a center and B is a saddle point. Figures 1 and 2 show the phase portrait for these cases.
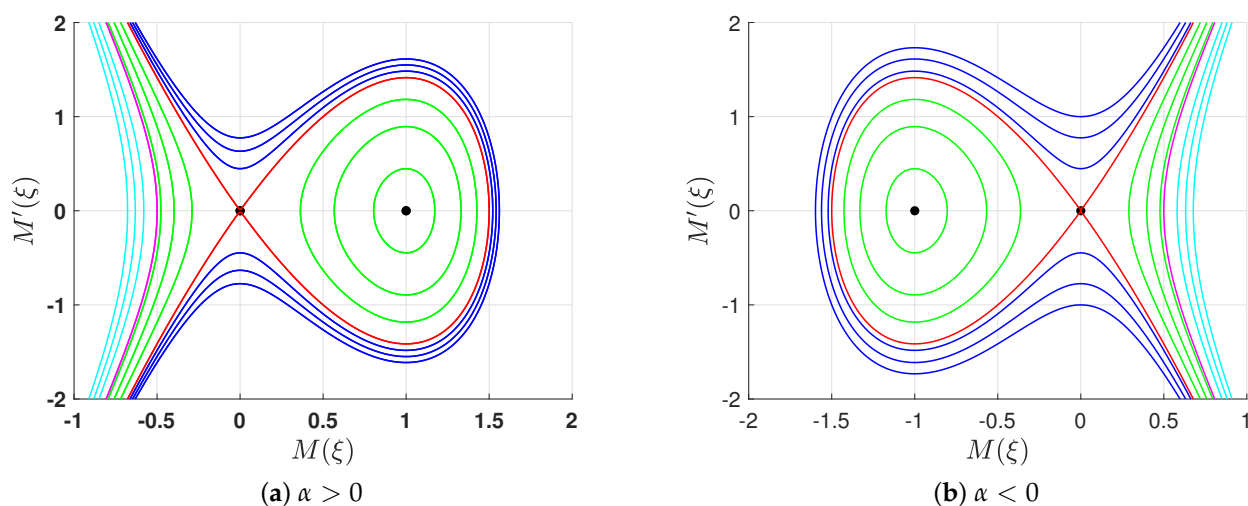

(a) $\alpha > 0$

(b) $\alpha < 0$

Figure 1. Phase portrait for the system (9) for $\beta > 0$. The black solid circles indicate the equilibrium points.

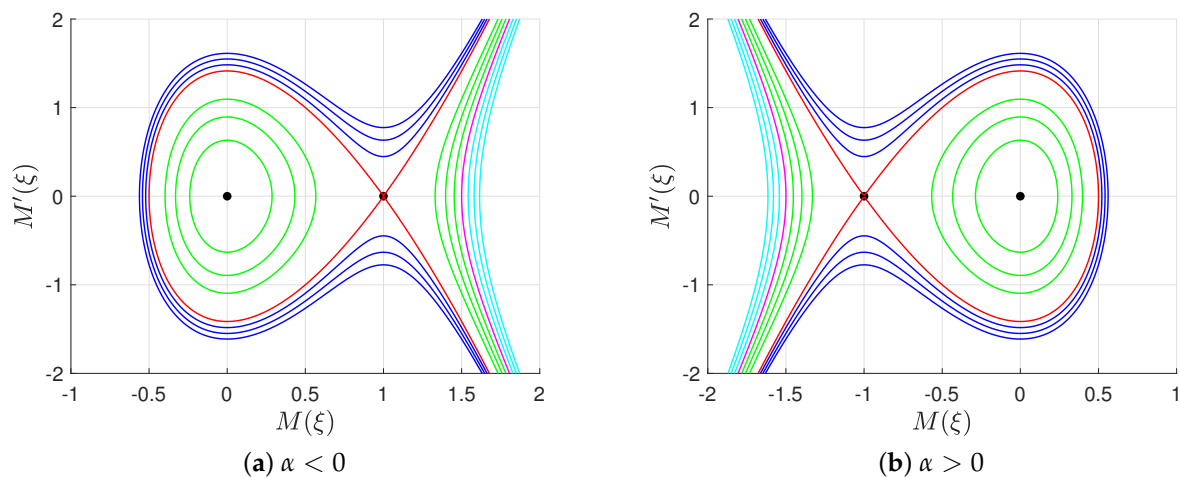**(a)** $\alpha < 0$ **(b)** $\alpha > 0$

Figure 2. Phase portrait for the system (9) for $\beta < 0$. The black solid circles indicate the equilibrium points.

To describe the phase portrait, we need the value of the constant of motion at the equilibrium points A and B. These are

$$f_0 = H(A) = 0, f_1 = H(B) = -\frac{4\beta^3}{27\alpha^2}. \tag{16}$$

The phase orbits are the energy levels parameterized by f, i.e.,

$$\mathcal{F}_f = \left\{ (M, N) \in \mathbb{R} \times \mathbb{R} : N^2 = \mathcal{W}_3(M) \right\}, \tag{17}$$

where $\mathcal{W}_3(M)$ is given by (14). In the following, we provide a brief description of the phase portraits depicted in Figures 1 and 2, respectively.

(A) Figure 1a illustrates the phase portrait corresponding to the system (9) when $(\alpha, \beta) \in \mathbb{R}^+ \times \mathbb{R}^+$. In this figure, we see a family of unbounded blue orbits $\mathcal{F}_{f > f_0}$. At $f = f_0$, the homoclinic red orbit emerges, connecting the saddle equilibrium point A with itself, in addition to two unbounded solutions. When $f \in (f_1, f_0)$, there are two families of orbits in green, denoted as $\mathcal{F}_f$. One of them is periodic, positioned inside the homoclinic orbit, while the other is unbounded, lying outside the homoclinic orbit. When $f = f_1$, there is an unbounded orbit in pink and the equilibrium solution at B, and when $f < f_1$, there is a family of unbounded orbits in cyan. The homoclinic orbit and the unbounded pink orbit are referred to as limiting orbits since the other orbits approach them as the value of f changes. This is called the degeneracy process. The periodic family of green orbits approaches the homoclinic orbit as $f \to 0^-$. Similarly, the family of unbounded blue orbits also approaches the homoclinic red orbit as $f \to 0^+$. A similar description applies to Figure 1b.

(B) When $(\alpha, \beta) \in \mathbb{R}^- \times \mathbb{R}^-$, the phase portrait for system (9) is shown in Figure 2a. For $f \in (f_1, \infty)$, there is a family of unbounded orbits shown in blue. When $f = f_1$, system (9) has a homoclinic orbit in red, connecting the saddle point B with itself, in addition to two unbounded orbits. If $f \in (f_0, f_1)$, there are two families of green orbits: one is a bounded periodic family located inside the homoclinic orbit, while the other is unbounded and appears outside the homoclinic orbit. For $f = f_0$, there is a pink unbounded orbit and the equilibrium solution at A. For $f < f_0$, there is an unbounded family of cyan orbits. The two orbits $\mathcal{F}_{f=f_1}$ and $\mathcal{F}_{f=f_0}$ are termed limiting orbits and play an essential role in studying the degeneracy property of the solutions, as we will see later. A similar description applies to Figure 2b.

4. Solutions Formulation

In this section we obtain all possible solutions for Equation (1) by considering the bifurcation constraints on the parameters α and β, and consequently, on the parameter f. We consider each case separately.

For the case where $(\alpha, \beta) \in \mathbb{R}^+ \times \mathbb{R}^+$, we have the following:

(a) If $f > 0$, system (9) has unbounded orbit in blue intersecting the M-axis in a single point representing the only real root for the polynomial (14). The polynomial $\mathcal{W}_3$ can be written as $\mathcal{W}_3 = 2\alpha(r_1 - M)(M - r_2)(M - r_2^*)$, where $r_1 \in \mathbb{R}$, $r_2 \in \mathbb{C}$, and * is the complex conjugation. The real solution interval is $M \in (-\infty, r_1)$. Taking $M(0) = r_1$ and integrating both sides of Equation (13), we obtain

$$M(\xi) = A_1 + r_1 - \frac{2A_1}{1 + \mathrm{cn}\left(\sqrt{2A_1\alpha}\xi, k_1\right)}, \tag{18}$$

where $A_1^2 = (\mathrm{Re}\, r_2 - r_1)^2 + \mathrm{Im}\, r_2)^2$, $k_1^2 = \frac{1}{2A_1}[A_1 + r_1 - \mathrm{Re}\, r_2]$. By employing the transformation (3), we obtain a new solution for Equation (2) in the form

$$\mathcal{Q}(x,t) = \left[A_1 + r_1 - \frac{2A_1}{1 + \mathrm{cn}\left(\sqrt{2A_1\alpha}\left(\frac{kx^p}{\Gamma(p+1)} + \omega t\right), k_1\right)}\right] e^{\rho \mathbb{H}(t) - \frac{\rho^2}{2}t}. \tag{19}$$

(b) If $f = f_0 = 0$, there is a homoclinic orbit in red and two unbounded orbits as illustrated in Figure 1a. Substituting $f = 0$ in (14), we obtain $M = 2\alpha M^2\left(\frac{\beta}{\alpha} - M\right)$. The real solution intervals are $(-\infty, 0)$ and $\left(0, \frac{\beta}{\alpha}\right)$. We examine each interval separately.

1. The interval $\left(0, \frac{\beta}{\alpha}\right)$ corresponds to the homoclinic orbit in red (see Figure 1a); we assume $M(0) = \frac{\beta}{\alpha}$ and integrate both sides of Equation (13) to obtain

$$M(\xi) = \frac{\beta}{\alpha} \, \mathrm{sech}^2\left(\sqrt{\frac{\beta}{2}}\xi\right). \tag{20}$$

Inserting the last expression into (3), we obtain

$$\mathcal{Q}(x,t) = \frac{\beta}{\alpha} \, \mathrm{sech}^2\left(\sqrt{\frac{\beta}{2}}\left(\frac{kx^p}{\Gamma(p+1)} + \omega t\right)\right) e^{\rho \mathbb{H}(t) - \frac{\rho^2}{2}t}, \tag{21}$$

which is a new solution for the SFLRW Equation (2).

2. The interval $(-\infty, 0)$ corresponds to the unbounded orbits in red (see Figure 1a). We assume $M(0) = -\infty$ and integrate both sides of Equation (13) to obtain

$$M(\xi) = -\frac{\beta}{\alpha} \, \mathrm{csch}^2\left(\sqrt{\frac{\beta}{2}}\xi\right). \tag{22}$$

Utilizing the transformation (3), we obtain a new solution for the SFLRW Equation (2) in the form

$$\mathcal{Q}(x,t) = -\frac{\beta}{\alpha} \, \mathrm{csch}^2\left(\sqrt{\frac{\beta}{2}}\left(\frac{kx^p}{\Gamma(p+1)} + \omega t\right)\right) e^{\rho \mathbb{H}(t) - \frac{\rho^2}{2}t}. \tag{23}$$

(c) For $f \in (f_1, 0)$, the system (9) has two different types of orbits in green, as shown in Figure 1a. These orbits intersect the M-axis at three points, namely, the real zeros of the polynomial (14). Hence, $\mathcal{W}_3(M) = 2\alpha(r_4 - M)(M - r_5)(M - r_6)$, where $r_4 <$

$0 < r_5 < r_6$. The real solution intervals are $M \in (r_5, r_6) \cup (-\infty, r_4)$. We obtain the solutions for each of these intervals separately.

1. The interval (r_5, r_6) corresponds to periodic orbits; we assume $M(0) = r_6$ and integrate both sides of Equation (13) to obtain

$$M(\xi) = r_6 - (r_6 - r_5)\, \text{sn}^2\left(\sqrt{\frac{\alpha}{2}(r_6 - r_4)}\xi, k_2 \right), \qquad (24)$$

where $k_2 = \sqrt{\frac{r_6 - r_5}{r_6 - r_4}}$. Using expression (3), we obtain

$$\mathcal{Q}(x, t) = \left[r_6 - (r_6 - r_5)\, \text{sn}^2\left(\sqrt{\frac{\alpha}{2}(r_6 - r_4)} \left(\frac{kx^p}{\Gamma(p+1)} + \omega t \right), k_2 \right) \right] e^{\rho \mathbb{H}(t) - \frac{\rho^2}{2}t}, \qquad (25)$$

which gives a novel solution for the SFRLW Equation (2).

2. The interval $(-\infty, r_4)$ corresponds to unbounded orbits in green as shown in Figure 1a. Assuming $M(0) = -\infty$ and integrating both sides of Equation (13), we obtain

$$M(\xi) = r_6 - (r_6 - r_4)\, \text{ns}^2\left(\sqrt{\frac{\alpha}{2}(r_6 - r_5)}\xi, k_2 \right). \qquad (26)$$

Substituting the last expression in (3), we obtain a new wave solution for the SFRLW Equation (1) in the form

$$\mathcal{Q}(x, t) = \left[r_6 - (r_6 - r_4)\, \text{ns}^2\left(\sqrt{\frac{\alpha}{2}(r_6 - r_5)} \left(\frac{kx^p}{\Gamma(p+1)} + \omega t \right), k_2 \right) \right] e^{\rho \mathbb{H}(t) - \frac{\rho^2}{2}t}, \qquad (27)$$

which agrees with solution (23).

(d) When $f = f_1$, in addition to the equilibrium solution at B, the system (9) has an unbounded pink orbit intersecting the M-axis in exactly one point. Hence, the polynomial (14) is written as $\mathcal{W}_3 = 2\alpha(r_6 - M)(M - r_7)(M - r_7^*)$, where $r_6 \in \mathbb{R}$ and $r_7 \in \mathbb{C}$. Assuming $M(0) = r_6$ and integrating both sides of Equation (13), we obtain

$$M(\xi) = A_2 + r_6 + \frac{2A_2}{1 + \text{cn}\left(\sqrt{2A_2\alpha}\xi, k_3 \right)}, \qquad (28)$$

where $A_2^2 = (\text{Re}r_7 - r_6)^2 + (\text{Im}r_7)^2$, $k_3^2 = \frac{1}{2A_2}[A_2 + r_6 - \text{Re}r_7]$. Using the transformation (3), a new solution for the SFLRW Equation (2) is constructed, given by

$$\mathcal{Q}(x, t) = \left[A_2 + r_6 + \frac{2A_2}{1 + \text{cn}\left(\sqrt{2A_2\alpha}\left(\frac{kx^p}{\Gamma(p+1)} + \omega t \right), k_3 \right)} \right] e^{\rho \mathbb{H}(t) - \frac{\rho^2}{2}t}. \qquad (29)$$

(e) For $f \in (-\infty, f_1)$, the system (9) has one of the unbounded orbits shown in cyan. The solutions corresponding to these orbits take the form in Equation (29), with different arguments.

The following lemma is crucial for constructing the solutions.

Lemma 1. *The dynamical system (9) is invariant under the following transformations:*

i. $(\alpha, \beta) \to (-\alpha, \beta), (M, N) \to (-M, -N)$,

ii. $(\alpha, \beta) \to (-\alpha, -\beta), (M, N) \to \left(\frac{2\beta}{3\alpha} - M, N \right)$,

iii. $(\alpha, \beta) \to (\alpha, -\beta), (M, N) \to \left(M - \frac{2\beta}{3\alpha}, N \right)$.

Finding solutions for the SFRLW Equation (2) is equivalent to solving the dynamical system (9). Thus Lemma 1 can be used to obtain the solutions depicted in Figures 1b and 2a,b from (19), (21), (23), (25), (27), and (29).

Remark 1.

1. *By setting $\rho = 0$, the solutions (19), (21), (23), (25), (27), and (29) give new solutions for the deterministic version of Equation (2) (FLRLW).*
2. *By setting $p = 1$, the solutions (19), (21), (23), (25), (27), and (29) give new solutions for the stochastic version of Equation (2) (SLRLW) with integer-order derivatives.*
3. *By setting $p = 1$ and $\rho = 0$, the solutions (19), (21), (23), (25), (27), and (29) give new solutions for the deterministic Equation (2) (RLW) with integer-order derivatives.*

Solution Degeneracy

In this section, we examine the consistency of the solutions obtained above by studying their degeneracy through the transition between phase plane orbits.

(a) The family of periodic orbits in green shown in Figure 1a approaches the homoclinic orbit in red as the parameter f approaches zero. Thus, we can obtain the homoclinic solution by taking $r_4 = r_5 = 0$ and $r_6 = \frac{\beta}{\alpha}$, and the solution (25) becomes

$$
\begin{aligned}
\mathcal{Q}(x,t) &= \frac{\beta}{\alpha}\left[1 - \operatorname{sn}^2\left(\sqrt{\frac{\beta}{2}}\left(\frac{kx^p}{\Gamma(p+1)} + \omega t\right),1\right)\right]e^{\rho\mathbb{H}(t)-\frac{\rho^2}{2}t}, \\
&= \frac{\beta}{\alpha}\left[1 - \tanh^2\left(\sqrt{\frac{\beta}{2}}\left(\frac{kx^p}{\Gamma(p+1)} + \omega t\right)\right)\right]e^{\rho\mathbb{H}(t)-\frac{\rho^2}{2}t}, \\
&= \frac{\beta}{2}\operatorname{sech}^2\left(\sqrt{\frac{\beta}{2}}\left(\frac{kx^p}{\Gamma(p+1)} + \omega t\right)\right)e^{\rho\mathbb{H}(t)-\frac{\rho^2}{2}t},
\end{aligned}
\tag{30}
$$

which agrees with solution (21). Likewise, the family of unbounded orbits in green will approach the unbounded orbit in pink when f approaches zero. Hence, for the later orbit, the solution in (27) becomes

$$
\begin{aligned}
\mathcal{Q}(x,t) &= \frac{\beta}{\alpha}\left[1 - \operatorname{ns}^2\left(\sqrt{\frac{\beta}{2}}\left(\frac{kx^p}{\Gamma(p+1)} + \omega t\right),1\right)\right]e^{\rho\mathbb{H}(t)-\frac{\rho^2}{2}t}, \\
&= \frac{\beta}{\alpha}\left[1 - \coth^2\left(\sqrt{\frac{\beta}{2}}\left(\frac{kx^p}{\Gamma(p+1)} + \omega t\right)\right)\right]e^{\rho\mathbb{H}(t)-\frac{\rho^2}{2}t}, \\
&= -\frac{\beta}{\alpha}\operatorname{csch}^2\left(\sqrt{\frac{\beta}{2}}\left(\frac{kx^p}{\Gamma(p+1)} + \omega t\right)\right)]e^{\rho\mathbb{H}(t)-\frac{\rho^2}{2}t}.
\end{aligned}
\tag{31}
$$

(b) When f tends to 0, the family of unbounded orbits in blue approaches the homoclinic orbit in red, as shown in Figure 1a. Therefore, we can obtain the solution by taking $r_1 = \frac{\beta}{\alpha}$ and $r_2 = r_2^* = 0$, resulting in the solution given by Equation (19), becoming

$$
\begin{aligned}
\mathcal{Q}(x,t) &= \frac{2\beta}{\alpha}\left[1 - \frac{1}{1 + \operatorname{cn}\left(\sqrt{\beta}\left(\frac{kx^p}{\Gamma(p+1)} + \omega t\right),1\right)}\right]e^{\rho\mathbb{H}(t)-\frac{\rho^2}{2}t}, \\
&= \frac{2\beta}{\alpha}\left[1 - \frac{1}{1 + \operatorname{sech}\left(\sqrt{\beta}\left(\frac{kx^p}{\Gamma(p+1)} + \omega t\right),1\right)}\right]e^{\rho\mathbb{H}(t)-\frac{\rho^2}{2}t}, \\
&= \frac{2\beta}{\alpha\left[1 + \cosh(\sqrt{2\beta}\xi)\right]} = \frac{\beta}{\alpha}\operatorname{sech}^2\sqrt{\frac{\beta}{2}}\xi,
\end{aligned}
\tag{32}
$$

which is consistent with the solution given in Equation (21).

This subsection demonstrates the correctness of the solutions and their consistency.

5. Physical Interpretations

In this section, we aim to study some of the solutions obtained previously, especially the ones in (21) and (25). We will investigate the distinct effects of fractional order and noise on these solutions, both separately and in combination.

We illustrate the solutions of the equations with fractional derivatives and/or varying levels of noise with $2D$ and $3D$ graphics generated using Mathematica.

Let us assume $m = 0.1, n = 0.4$. Equation (2) becomes

$$\mathrm{d}\mathcal{Q} + \left[\mathbb{T}_x^p \mathcal{Q} - 0.05 \mathcal{Q} \mathbb{T}_x^p \mathcal{Q}\right]\mathrm{d}t - 0.4\mathbb{T}_x^{2p}\mathrm{d}\mathcal{Q} = \rho \mathcal{Q}\mathrm{d}\mathbb{H}. \tag{33}$$

Let us assume that Equation (33) has a solution of the form (3) with $\omega = 2$ and $k = 10$. Using Equation (8), we obtain $\alpha = 0.01041666667$ and $\beta = 0.07500000000$. Since $\alpha > 0$ and $\beta > 0$, Equation (33) has solutions given by (19), (21), (23), (25), (27), and (29).

We examine these solutions in each interval with real solutions.

1. For $f = -0.25 \in (f_1, 0) = (-0.5759999997, 0)$, Equation (33) has a solution (25) which is given by

$$\mathcal{Q}(x,t) = [6.658708455 - 4.470368312\,\mathrm{sn}^2(\frac{1.525882312x^p}{\Gamma(p+1)}$$
$$+ 0.3051764624t, 0.7336383764)]e^{\rho\mathbb{H}(t) - \frac{\rho^2}{2}t}. \tag{34}$$

Figure 3 illustrates *the impact of noise* on the solution (34) for Equation (33) with an integer-order derivative, i.e., $p = 1$. Figure 3a shows that the solution, shown in blue, is periodic in the deterministic case (when $\rho = 0$). As the strength of the noise ρ increases, both the amplitude and the width of the solution decrease. The surface of the solution (34) is initially periodic and smooth; however, as the noise strength increases, it nearly loses its periodicity and becomes somewhat rough.
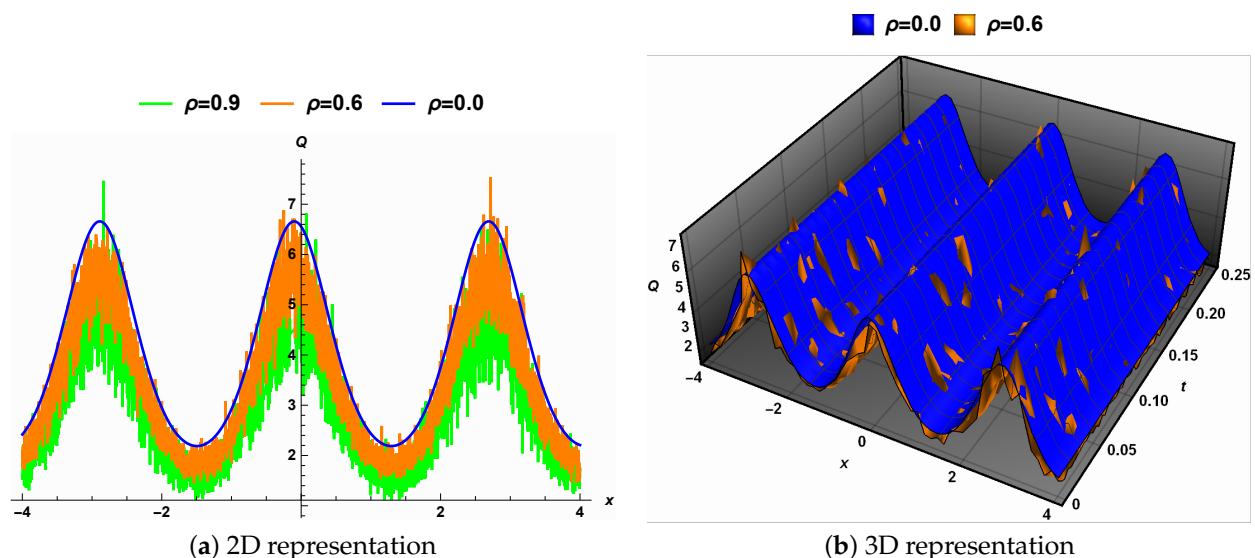

(**a**) 2D representation   (**b**) 3D representation

Figure 3. The impact of the noise strength on the solution (34) with $p = 1$ and different values of the noise strength ρ.

Figure 4 shows the impact of fractional derivatives on the solution (34) for Equation (33) in the deterministic case, i.e., when $\rho = 0$. The 2D representation in Figure 4a shows that

the solution, shown in blue, is periodic when $p = 1$. As the fractional order p decreases, the solutions remain periodic, but the period lengthens. Meanwhile, the solution's amplitude stays nearly constant, but its width expands as p decreases. Figure 4b shows that the surface depicting the solution (34) is periodic and smooth for all possible values of the fractional order p.
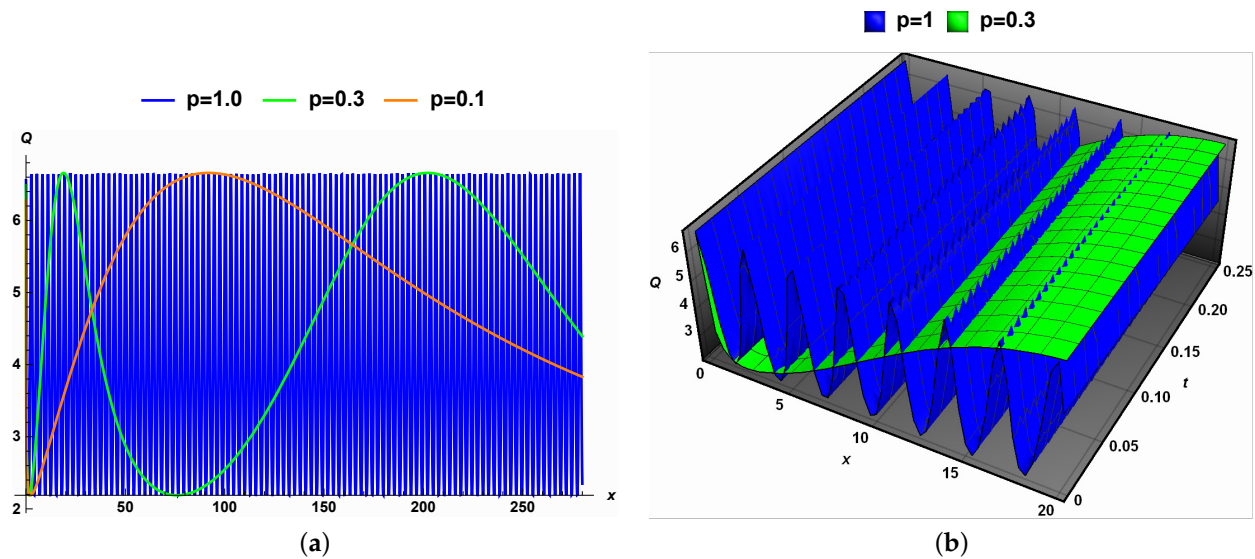

Figure 4. The effects of the fractional order p on the solution (34) in the deterministic case with different values of the fractional order p.

Figure 5 shows the combined influence of noise strength and using fractional-order derivatives on the solution (34). As shown in Figure 5a, the solution is periodic in the classical case ($\rho = 0, p = 1$). However, as the fractional order diminishes and the noise grows, the solution remains approximately periodic, but its period increases significantly. Its amplitude remains approximately constant and its width increases. The surface depicting the solution (34) (Figure 5b) is periodic and smooth in the classical case ($p = 1, \rho = 0$) but loses its smoothness as the noise strength increases.
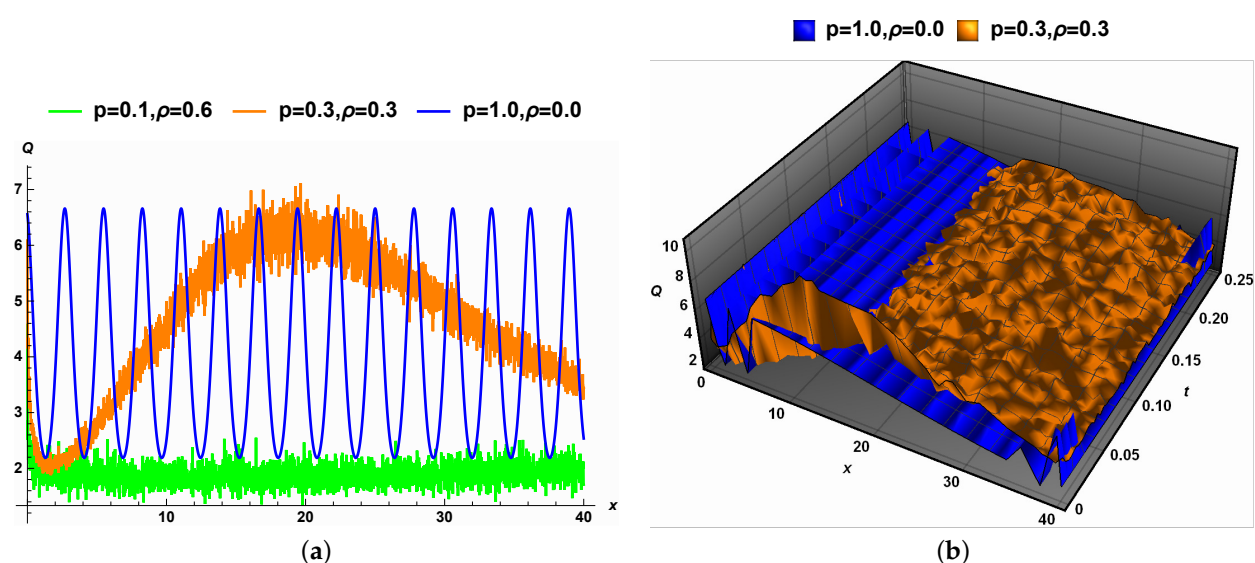

Figure 5. The combined effect of the fractional order p and the noise strength ρ on the solution (34).

2. When $f = 0$, Equation (33) admits a solution of the form (21):

$$\mathcal{Q}(x,t) = 7.199999998 \operatorname{sech}^2\left(\frac{1.936491673 x^p}{\Gamma(p+1)} + 0.3872983346\, t\right) e^{\rho \mathbb{H}(t) - \frac{\rho^2}{2}t}. \quad (35)$$

Figure 6a shows the effect of noise strength on the solution (35) to the SFLRW Equation (33) with integer derivatives. In the deterministic case, that is, in the absence of noise, the solution (35) is solitary, as shown in blue. As the noise level increases, the amplitude of the solution remains roughly the same, but its width decreases. Figure 6b displays the surface depicting the solution (35) in the deterministic case. The solution is symmetric and smooth. However, as the noise increases, this surface becomes rough and loses its symmetry.
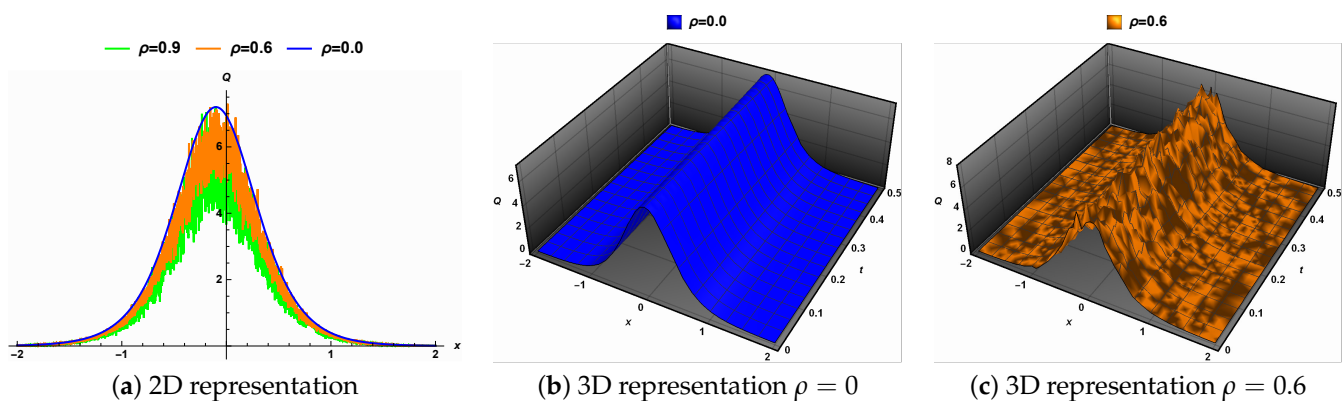

(**a**) 2D representation (**b**) 3D representation $\rho = 0$ (**c**) 3D representation $\rho = 0.6$

Figure 6. The effect of the noise strength on the solution (35) with $p = 1$ and different values of the noise strength ρ.

Figure 7 illustrates the influence of the fractional order p on the solution (35) in the absence of noise, i.e., $\rho = 0$. Figure 7a shows the solution is solitary and symmetric when the fractional-order derivative is one. As the fractional order decreases from one, the solution loses its symmetry and both its amplitude and width decrease. Figure 7b shows the surface representing the solution (35). This surface is smooth and symmetric when $p = 1$ and loses its symmetry as the order of fractional derivatives decreases.
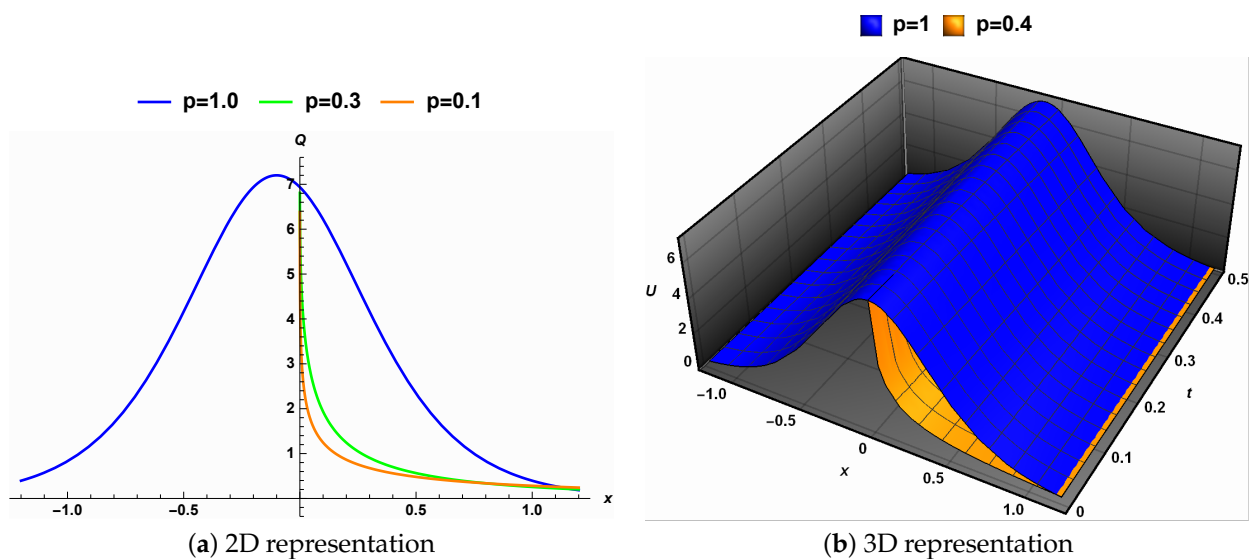

(**a**) 2D representation (**b**) 3D representation

Figure 7. The impact of the fractional order p on the solution (34) in the deterministic case with different values of the fractional order p.

Figure 8 illustrates how the solution (35) for the SFLRW Equation (33) is influenced by both the strength of noise and fractional derivatives. Figure 8a shows the solution as solitary and symmetric in the classical case, i.e., when $p = 1$ and $\rho = 0$. As the fractional derivative order declines and the intensity of noise increases, the solution loses its symmetry, and its amplitude decreases. The surface representing the solution (35) is symmetric and smooth in the classical case. However, it becomes rough and non-smooth as the order of fractional derivatives decreases from one and the noise strength increases.
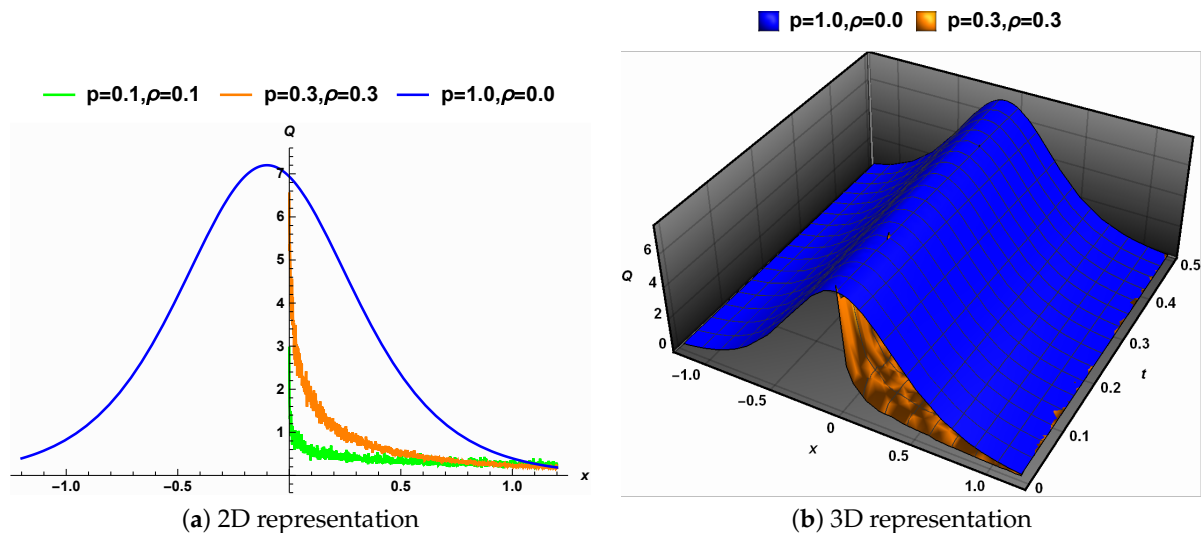

(**a**) 2D representation

(**b**) 3D representation

Figure 8. The combined effect of the fractional order p and the noise strength ρ on the solution (34).

6. Conclusions

This study explores how spatial fractional derivatives and the multiplicative Wiener process affect analytical solutions of the $(1 + 1)$-dimensional regularized long wave equation. We introduce new solutions of this equation and study their bifurcation. These solutions are also new for the deterministic version of Equation (2), with fractional- or integer-order derivatives, and for the stochastic version of Equation (2) with integer-order derivatives. The utilization of bifurcation theory offers several advantages. It allows us to construct real solutions only by introducing the concept of intervals of real propagation. When the parameters are fixed, there are multiple intervals of real wave propagation. The solutions corresponding to each interval differ significantly from the mathematical and physical perspectives. Thus, e.g., for $(\alpha, \beta) \in \mathbb{R}^+ \times \mathbb{R}^+$ and $f \in (f_1, 0)$, there are two intervals of real propagation. One of them is (r_5, r_6), a bounded interval where the corresponding solution (25) is bounded and periodic, while the other is unbounded $(-\infty, r_4)$ with the corresponding solution (29) being unbounded. The utilization of these intervals of real propagation is essential to the study of the solution. The exact solutions obtained can be used to characterize a wide range of properties in the evolution of long waves. We graphically explored the influence of fractional derivative orders and noise strength, both separately and in combination, on some of the obtained solutions. These effects are evident in the width, amplitude, smoothness, and periodicity of the solutions. Moreover, the smooth surface of the solution in the deterministic case was roughened by the introduction of a noise term and lost its periodicity as a consequence of the fractional-order derivatives.

This work offers several options for researchers desiring to advance the topic by exploring Equation (2) in the presence of additive noise and conducting numerical investigations to support our findings.

Author Contributions: Conceptualization, M.A.N. and A.A.; methodology, M.A.N., B.A., and A.A.; software, B.A. and A.A.; formal analysis, B.A. and M.A.N.; investigation, A.A. and M.A.N.; writing—original draft preparation, B.A. and M.A.N.; writing—review and editing, B.A. and A.A.; visualization,

Appendix A. Jumarie's Modified Riemann–Liouville Derivative and Standard Wiener Process

Definition A1 ([38]). *Let $f : \mathbb{R} \to \mathbb{R}$ be a function and $p \in \mathbb{R}$ the fractional derivative of f of order p in the sense of Jumarie's modified Riemann–Liouville form, defined as*

$$
\mathbb{T}_t^p(f)(t) = \begin{cases} \frac{1}{\Gamma(-p)} \frac{d}{dt} \int_0^t (t-s)^{-p-1}[f(s) - f(0)]ds, & p < 0 \\[2mm] \frac{1}{\Gamma(1-p)} \frac{d}{dt} \int_0^t (t-s)^{-p}[f(s) - f(0)]ds, & 0 < p < 1 \\[2mm] \left(f^{(n)}(t) \right)^{(p-n)}, & n \le p < n+1, n \ge 1 \end{cases} \tag{A1}
$$

This modified Riemann–Liouville derivative has the following properties that will be used in this paper:

1. $\mathbb{T}_t^p(t^s) = \frac{\Gamma(1+s)}{\Gamma(1+s-p)} t^{s-p}$,
2. $\mathbb{T}_t^p f[u(t)] = f_u'[u(t)]\mathbb{T}_t^p u(t)$.

for any $p-$ differentiable function f, f_1, f_2 at t, in the sense of Jumarie's modified Riemann–Liouville form.

Definition A2 ([39]). *A Stochastic process $\{\mathbb{H}(t)\}_{t \ge 0}$ is a standard Wiener process if the following are true:*

1. $\mathbb{H}(0) = 0$,
2. $\mathbb{H}(t)$ *is a continuous function for $t \ge 0$,*
3. *For $t_3 < t_2 < t_1$, $\mathbb{H}(t_1) - \mathbb{H}(t_2)$ and $\mathbb{H}(t_2) - \mathbb{H}(t_3)$ are independent,*
4. $\mathbb{H}(t_2) - \mathbb{H}(t_1)$ *has a normal distribution with mean zero and variance $t_2 - t_1$.*

References

1. Peregrine, D.H. Calculations of the development of an undular bore. *J. Fluid Mech.* **1966**, *25*, 321–330. [CrossRef]
2. Benjamin, T.B.; Bona, J.L.; Mahony, J.J. Model equations for long waves in nonlinear dispersive systems. *Philos. Trans. R. Soc. London. Ser. A Math. Phys. Sci.* **1972**, *272*, 47–78. [CrossRef]
3. Bona, J.L.; Bryant, P.J. A mathematical model for long waves generated by wavemakers in non-linear dispersive systems. *Math. Proc. Camb. Philos. Soc.* **1973**, *73*, 391–405. [CrossRef]
4. Eilbeck, J.; McGuire, G. Numerical study of the regularized long-wave equation I: Numerical methods. *J. Comput. Phys.* **1975**, *19*, 43–57. [CrossRef]
5. El-Danaf, T.S.; Ramadan, M.A.; Abd Alaal, F.E. The use of adomian decomposition method for solving the regularized long-wave equation. *Chaos Solitons Fractal.* **2005**, *26*, 747–757. [CrossRef]
6. Pshtiwan, O.M.; Alqudah, M.A.; Hamed, Y.S.; Kashuri, A.; Abualnaja, K.M. Solving the Modified Regularized Long Wave Equations via Higher Degree B-Spline Algorithm. *J. Funct. Spaces* **2021**, *2021*, 5580687. [CrossRef]
7. Hirsch, M.W.; Smale, S.; Devaney, R.L. *Differential Equations, Dynamical Systems, and an Introduction to Chaos*; Academic Press: Cambridge, MA, USA; Elsevier: Amsterdam, The Netherlands, 2013. [CrossRef]
8. Farlow, S. *Partial Differential Equations for Scientists and Engineers*; Dover Publications: Mineola, NY, USA, 1993.

9. Zhou, Y. *Fractional Evolution Equations and Inclusions: Analysis and Control*; Academic Press: Cambridge, MA, USA; Elsevier: Amsterdam, The Netherlands, 2016. [CrossRef]

10. Kubica, A.; Ryszewska, K.; Yamamoto, M. *Time-Fractional Differential Equations, A Theoretical Introduction*; Springer: Singapore, 2020. [CrossRef]

11. Tarasov, V.E. *Fractional Dynamics: Applications of Fractional Calculus to Dynamics of Particles, Fields and Media*; Springer: Berlin/Heidelberg, Germany, 2010. [CrossRef]

12. AL Nuwairan, M. The exact solutions of the conformable time fractional version of the generalized Pochhammer–Chree equation. *Math. Sci.* **2023**, *17*, 305–316. [CrossRef]

13. Magin, R.L. Fractional calculus models of complex dynamics in biological tissues. *Comput. Math. Appl.* **2010**, *59*, 1586–1593, Fractional Differentiation and Its Applications. [CrossRef]

14. Butt, A.; Imran, M.; Batool, S.; AL Nuwairan, M. Theoretical Analysis of a COVID-19 CF-Fractional Model to Optimally Control the Spread of Pandemic. *Symmetry* **2023**, *15*, 380. [CrossRef]

15. Braumann, C.A. *Introduction to Stochastic Differential Equations with Applications to Modelling in Biology and Finance*; Wiley: Hoboken, NJ, USA, 2019. [CrossRef]

16. Baxendale, P.; Lototsky, S.V. *Stochastic Differential Equations: Theory and Applications*; World Scientific: Singapore, 2007. [CrossRef]

17. Evans, L.C. *An Introduction to Stochastic Differential Equations*; American Mathematical Society: Providence, RI, USA, 2013.

18. Swishchuk, A. *Random Evolutions and Their Applications: New Trends*; Springer Science & Business Media: Berlin/Heidelberg, Germany, 2013; Volume 504.

19. Weinan, E.; Li, X.; Vanden-Eijnden, E. Some recent progress in multiscale modeling. In *Multiscale Modelling and Simulation*; Springer: Berlin/Heidelberg, Germany, 2004; pp. 3–21.

20. Kamrani, M. Numerical solution of stochastic fractional differential equations. *J. Fluid Mech.* **2015**, *68*, 81–93. [CrossRef]

21. Ha, T.; Li, Z.; Kun, K. Exact solutions of the stochastic fractional long–short wave interaction system with multiplicative noise in generalized elastic medium. *Results Phys.* **2023**, *44*, 106174. [CrossRef]

22. Al Nuwairan, M. Bifurcation and Analytical Solutions of the Space-Fractional Stochastic Schrödinger Equation with White Noise. *Fractal Fract.* **2023**, *7*, 157. [CrossRef]

23. Yang, M. Existence uniqueness of mild solutions for Ψ-Caputo fractional stochastic evolution equations driven by fBm. *J. Inequal. Appl.* **2021**, *2021*, 170. [CrossRef]

24. Yuan, C.; Mao, X. Convergence of the Euler–Maruyama method for stochastic differential equations with Markovian switching. *Math. Comput. Simul.* **2004**, *64*, 223–235. [CrossRef]

25. Elbrolosy, M.; Alhamud, M.; Elmandouh, A. Analytical solutions to the fractional stochastic (3 + 1) equation of fluids with gas bubbles using an extended auxiliary function method. *Alex. Eng. J.* **2024**, *92*, 254–266. [CrossRef]

26. Mohammed, W.W.; Cesarano, C.; Elmandouh, A.A.; Alqsair, I.; Sidaoui, R.; Alshammari, H.W. Abundant optical soliton solutions for the stochastic fractional fokas system using bifurcation analysis. *Phys. Scr.* **2024**, *99*, 045233. [CrossRef]

27. Li, S.; Khan, S.; Riaz, M.; AlQahtani, S.A.; Alamri, M.M. Numerical simulation of a fractional stochastic delay differential equations using spectral scheme: A comprehensive stability analysis. *Sci. Rep.* **2024**, *14*, 6930. [CrossRef]

28. Maarouf, N.; Maadan, H.; Hilal, K. Lie symmetry analysis and explicit solutions for the time-fractional regularized long-wave equation. *Int. J. Differ. Equ.* **2021**, *2021*, 6614231. [CrossRef]

29. Kumar, D.; Singh, J.; Baleanu, D.; Sushila. Analysis of regularized long-wave equation associated with a new fractional operator with Mittag-Leffler type kernel. *Phys. A Stat. Mech. Its Appl.* **2018**, *492*, 155–167. [CrossRef]

30. Jhangeer, A.; Muddassar, M. andKousar, M.; Infal, B. Multistability and Dynamics of Fractional Regularized Long Wave equation with Conformable Fractional Derivatives. *Ain Shams Eng. J.* **2021**, *12*, 2153–2169. [CrossRef]

31. Al-Askar, F.M.; Cesarano, C.; Mohammed, W.W. Effects of the wiener process and beta derivative on the exact solutions of the kadomtsev–petviashvili equation. *Axioms* **2023**, *12*, 748. [CrossRef]

32. Mohammed, W.W.; Alshammari, M.; Cesarano, C.; Albadrani, S.; El-Morshedy, M. Brownian motion effects on the stabilization of stochastic solutions to fractional diffusion equations with polynomials. *Mathematics* **2022**, *10*, 1458. [CrossRef]

33. Kilbas, A.A.; Srivastava, H.M.; Trujillo, J.J. *Theory and Applications of Fractional Differential Equations*; Elsevier: Amsterdam, The Netherlands, 2006.

34. Goldstein, H. *Classical Mechanics*; Addison-Wesley Series in Physics; Addison-Wesley USA: Boston, MA, USA, 1980.

35. Saha, A.; Banerjee, S. *Dynamical Systems and Nonlinear Waves in Plasmas*; CRC Press: Boca Raton, FL, USA, 2021; p. x+207.

36. Nemytskii, V.V. *Qualitative Theory of Differential Equations*; Princeton University Press: Princeton, NJ, USA, 2015; Volume 2083.

37. Hand, L.N.; Finch, J.D. *Analytical Mechanics*; Cambridge University Press: Cambridge, UK, 1998.

38. Jumarie, G. Modified Riemann-Liouville derivative and fractional Taylor series of nondifferentiable functions further results. *Comput. Math. Appl.* **2006**, *51*, 1367–1376. [CrossRef]

39. Platen, E.; Bruti-Liberati, N. *Numerical Solution of Stochastic Differential Equations with Jumps in Finance*; Springer Science & Business Media: Berlin/Heidelberg, Germany, 2010; Volume 64.